JACS
JOURNAL OF THE AMERICAN CHEMICAL SOCIETY
Article
pubs.acs.org/JACS

Glutamine Amide Flip Elicits Long Distance Allosteric Responses in the LOV Protein Vivid

Abir Ganguly,[†] Walter Thiel,[†] and Brian R. Crane*[,‡]

[†]Max-Planck-Institut für Kohlenforschung, Kaiser-Wilhelm-Platz 1 45470 Mülheim an der Ruhr, Germany
[‡]Department of Chemistry and Chemical Biology, Cornell University, Ithaca, New York 14853, United States

Supporting Information

ABSTRACT: Light-oxygen-voltage (LOV) domains sense blue light through the photochemical formation of a cysteinyl-flavin covalent adduct. Concurrent protonation at the flavin N5 position alters the hydrogen bonding interactions of an invariant Gln residue that has been proposed to flip its amide side chain as a critical step in the propagation of conformational change. Traditional molecular dynamics (MD) and replica-exchange MD (REMD) simulations of the well-characterized LOV protein Vivid (VVD) demonstrate that the Gln182 amide indeed reorients by ∼180° in response to either adduct formation or reduction of the isoalloxazine ring to the neutral semiquinone, both of which involve N5 protonation. Free energy simulations reveal that the relative free energies of the flipped Gln conformation and the flipping barrier are significantly lower in the light-adapted state. The Gln182 flip stabilizes an important hinge-bβ region between the PAS β-sheet and the N-terminal cap helix that in turn destabilizes an N-terminal latch region against the PAS core. Release of the latch, observed both experimentally and in the simulations, is known to mediate light-induced VVD dimerization. This computational study of a LOV protein, unprecedented in its agreement with experiment, provides an atomistic view of long-range allosteric coupling in a photoreceptor.

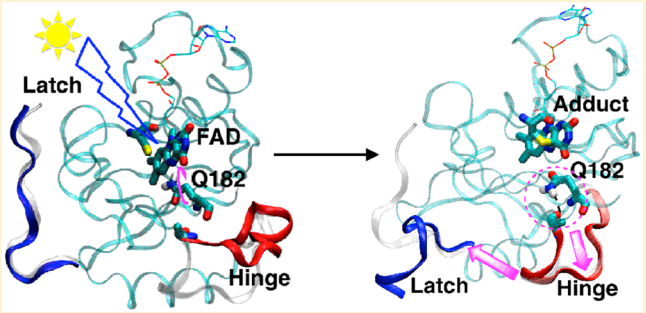

INTRODUCTION

Light-oxygen-voltage (LOV) domains are widespread light-sensing modules found throughout biology that are also of great use in optogenetics.[1−4] LOV domains are a subclass of PAS proteins (named for the representatives: **P**eriod, **A**ryl hydrocarbon receptor nuclear translocator, and **S**ingleminded) that utilize flavin cofactors as blue-light chromophores. In a highly conserved and well-studied mechanism, the excited triplet state of the isoalloxazine flavin ring reacts with an active site cysteine residue to form a covalent adduct between the Cys thiol and the flavin C4a position.[4−6] Concurrent protonation of the flavin N5 atom alters the hydrogen bonding of an invariant Gln residue that resides on the most C-terminal β-strand of the PAS domain fold.[7−10] More peripheral changes in conformation and hydrogen bonding relay the signal to the more variable Ncap and Ccap regions that pack against the β-sheet on the side opposite the flavin binding pocket.[1,3] Although the global conformational changes accompanying adduct formation vary depending on the LOV domain, the interactions involving the invariant flavin, Cys, and Gln moieties are likely to be similar, if not conserved.[1−4]

In the dark or resting state of the LOV domain the conserved Gln residue orients its amide nitrogen toward the unprotonated N5 of the flavin (Figure 1).[7,8,10−16] This interaction is destabilized when N5 is protonated upon the formation of the cysteinyl-flavin adduct. Crystallographic studies on several LOV proteins, including the fungal light sensor Vivid (VVD),[10,13] suggest that in the light-adapted adduct state the conserved Gln (182 in the case of VVD) flips its amide side chain to direct the carbonyl group toward the protonated flavin N5.[7,8,10,12−15] However, not all structures show the Gln flip[16,17] and in many instances the resolution is lacking to make definitive assignments of the side chain orientation. Other complications such as the influence of the crystal lattice on coupled conformational changes confound the interpretation. Nonetheless, mutational studies have shown that the conserved Gln residue is key for setting photocycle properties and sending conformational signals.[9,18−22] Infrared vibrational spectroscopy is consistent with the Gln flip in the adduct state, but resonances cannot be unambiguously assigned to the side chain itself.[20,23]

Light-induced oligomerization is critical for VVD to send signals in the fungal clock.[13] The structure of the VVD light-state dimer indicates that Gln182 reorientation affects hydrogen bonding to the first β-strand of the PAS domain (Aβ) and the hinge (residues 69−71) that links it to a β-strand region (bβ; residues 62−68) of the Ncap.[10,13,24] Changes in hinge hydrogen bonding shift bβ and destabilize the so-called N-terminal latch, the signal-initiating element of the Ncap, that

Received: October 12, 2016
Published: February 1, 2017

DOI: 10.1021/jacs.6b10701
J. Am. Chem. Soc. 2017, 139, 2972−2980

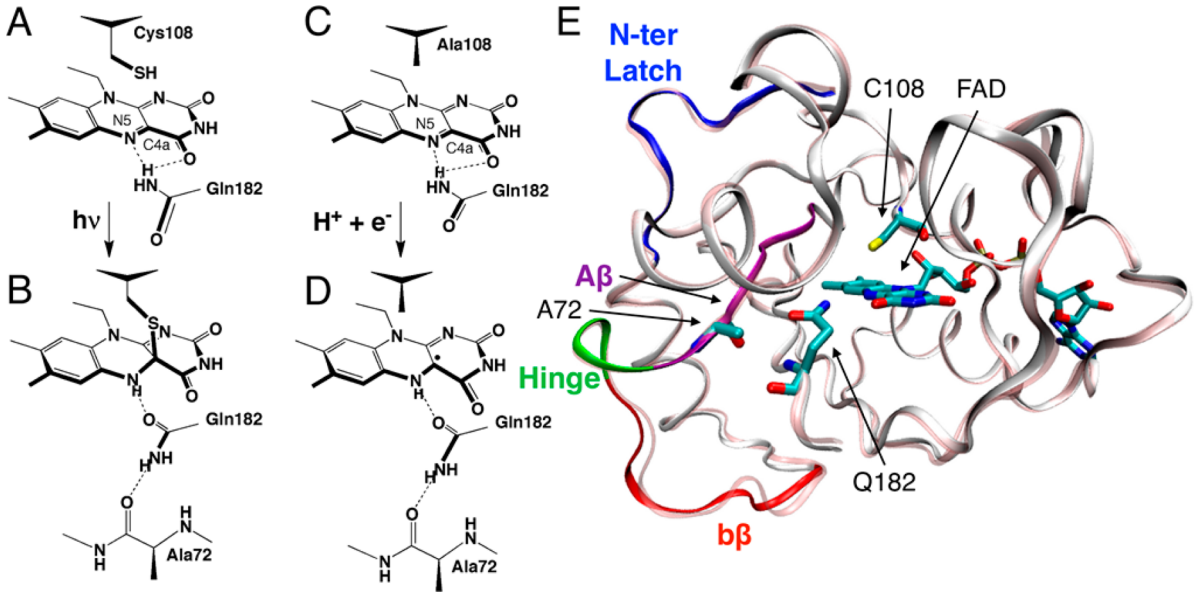

Figure 1. Photochemistry of the VVD LOV domain. In the dark state (A) Gln182 faces FAD with its amide. Upon illumination (B) a covalent bond forms between the Cys108 thiol and C4a of FAD causing protonation of flavin N5; this alters the hydrogen bonding pattern of Gln182 and promotes a flip of the side-chain amide to face FAD with its carbonyl group. Photoreduction of FAD in the absence of Cys108 (C) to a neutral semiquinone state containing protonated FAD N5 (D) can also trigger the Gln182 conformational switch. (E) Dark state crystal conformation of VVD with key residues and regions labeled [PDB ID 2PD7]. The light adapted protein conformation of VVD [PDB ID 2PDR] is shown for the backbone in pale pink.

otherwise encircles the protein to bind near the flavin binding pocket.[10,13] In the adduct-state dimer, the N-terminal latch has released from this position and binds into the hinge of the opposing subunit.[13]

Previous MD studies of phototropin LOV1 and LOV2 and of VVD do not reproduce the active site Gln flip[25,26] or report the N-terminal latch release. Instead, these studies reveal more dramatic alternations of the Gln side chain that, for VVD, are not found in the crystal structure of the fully activated light-state dimer.[13] Herein, we combine traditional all-atom MD simulations with explicit solvent, temperature replica exchange MD simulations and free energy simulations with a wealth of existing experimental data to paint an atomistic picture of the VVD conformational activation mechanism. We investigate three VVD states with different active site configurations representing the different stages of the VVD signaling pathway. The simulations recapitulate a 180° flip of the Gln182 side chain, as well as more peripheral conformational changes observed experimentally, including the release of the N-terminal latch. Furthermore, the simulations reveal an interesting inverse relationship between the motions of the VVD hinge-bβ region and of the N-terminal region. In a previous study a VVD variant in which the active site Cys has been changed to Ala was also found to signal after photoreduction of the flavin to the neutral semiquinone state, which also has N5 protonated.[19] In our simulations the Cys-less variant also gives rise to the Gln conformational switch and thus points to a similar conformational activation mechanism in the Cys-less variant. Finally, free energy simulations indicate that in the light state the barrier for Gln182 flipping is reduced and the flipped conformation is substantially stabilized.

METHODS

Molecular Dynamics Simulations. The MD simulations reported in this study were based on the dark (PDB ID: 2PD7) and light-adapted (PDB ID: 2PDR) crystal structures of VVD from *Neurospora crassa*.[10] In all simulations, the protonation states of the nonactive site histidine residues were determined by visual inspection of hydrogen bonding networks. Surface exposed His residues were assumed to be neutral. The protein was immersed in an orthorhombic box of rigid TIP3P waters[27] and Na^+ ions were added to neutralize the system. Additional Na^+ and Cl^- ions were added to produce a physiological salt concentration of 0.15 M. The solvated box was replicated in all three dimensions using periodic boundary conditions and long-range electrostatic interactions were calculated using the particle mesh Ewald (PME) method[28] with a cutoff of 12 Å and a grid spacing of 1 Å. The SHAKE algorithm[29] was used to constrain all bonds involving hydrogen. After equilibrating the system through several stages that held either pressure or volume constant and varied temperature, production trajectories of 25 ns were computed at 298 K in the canonical ensemble (i.e., constant NVT) using a 1 fs time step. A modified Nosé–Hoover thermostat[30] along with Langevin dynamics was employed to maintain constant pressure and temperature during the simulations.[31,32] All MD simulations were performed using the NAMD program[33] and the CHARMM22 force field[34] with the CMAP correction.[35]

To explore the dynamics of VVD along the early stages of its signal transduction pathway, we performed three independent sets of MD simulations with different active site configurations corresponding to three stages of VVD activation. The ground-state VVD simulations were based on the dark-state VVD crystal structure (PDB ID: 2PD7) (referred to in this study as DS simulations). The light-state VVD simulations were also based on the dark-state VVD crystal structure but with a covalent bond between C4A of the FAD chromophore and S of Cys108 and with a proton on the N5 atom (referred to in this study as LS simulations), while the light-adapted-state VVD simulations were based on the light-illuminated oxidized protein structure containing the cysteinyl adduct (as in LS) and also the local protein conformational changes that result from adduct formation (PDB ID: 2PDR) (referred to in this study as LAS simulations). A fourth set of MD simulations was carried out with the protein in the dark state and the FAD chromophore in the neutral semiquinone radical state (referred to this study as FADH simulations). For each VVD state we propagated at least three independent trajectories. The force field parameters of the neutral FAD were taken from a previous

DOI: 10.1021/jacs.6b10701
J. Am. Chem. Soc. 2017, 139, 2972–2980

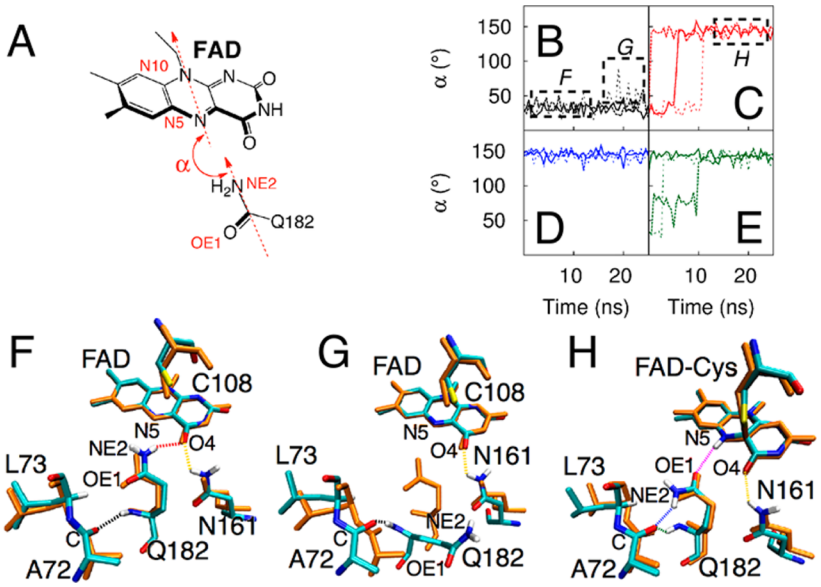

Figure 2. Conformation of Gln182 in various stages of the VVD photocycle. (A) Illustration of the angle α formed between the vector along the Gln182 amide bond and the vector passing through N5 and N10 of FAD; α is chosen as reaction coordinate to describe the orientation of Gln182. (B-E) Plots of α along the MD trajectories for the VVD states DS (B, black), LS (C, red), LAS (D, blue), and FADH (E, green), with different line styles corresponding to the three independent MD trajectories. (F−H) Representative snapshots from the trajectories in the regions marked by the dotted boxes F−H in the plots for DS (B) and LS(C). See text for discussion.

study,[36] while those of the cysteinyl-FAD adduct and the neutral radical FAD were obtained in a fashion similar to that study,[37] namely by first calculating the electrostatic potentials of the optimized molecules using *ab initio* quantum mechanical methods (Hartree−Fock, 6-31G* basis) and then subsequently fitting the respective electrostatic potentials to determine the charges on the atoms. The partial charges of neutral FAD were taken as initial guess in the fitting procedure; charges derived with a default initial guess were found to be qualitatively similar.

Replica Exchange Molecular Dynamics (REMD) Simulations. We carried out independent REMD simulations[38,39] for VVD in the DS, LS, LAS, and FADH states. In these simulations, 26 replicas were distributed between 300 to 350 K. The temperatures of the replicas were chosen to increase exponentially to obtain uniform acceptance ratios between neighboring replicas. A Web server was used to generate the temperatures for the replicas.[40] Each replica was equilibrated independently at its respective temperature; first under constant NVT conditions and then at constant NPT conditions for a total of 600 ps. Production trajectories were propagated under constant NPT conditions for 100 ns with a 2 fs time step. During the NPT simulations, constant temperature was maintained using the Nosé−Hoover thermostat[30] with a τ_t of 5 ps and constant pressure was maintained using the Parrinello−Rahman barostat[41,42] with isotropic pressure coupling, a τ_p of 5 ps and a compressibility of 4.5 $\times$ 10^{-5} bar^{-1}. As in the case of the traditional MD simulations, all bonds involving hydrogen atoms were constrained using the SHAKE algorithm,[29] long-range electrostatics were treated using the PME method[28] with a 12 Å cutoff and default grid dimensions (Fourier spacing of 1.2 Å and PME order of 4). Replica exchanges were attempted every 0.4 ps, which resulted in exchange probabilities between neighboring replicas of 20−30%. The REMD simulations were performed using the GROMACS software[43] and the CHARMM22 force field[34] with the CMAP correction.[35]

Cross-Correlation Analysis. To investigate correlated motions in VVD we calculated normalized covariance matrices, or dynamic cross-correlation matrices (DCCMs), from the MD and REMD trajectories, according to the following equation:

$$C_{ij} = \frac{\langle (x_i - \langle x_i \rangle)(x_j - \langle x_j \rangle) \rangle}{\sqrt{(\langle (x_i - \langle x_i \rangle)(x_i - \langle x_i \rangle) \rangle)(\langle (x_j - \langle x_j \rangle)(x_j - \langle x_j \rangle) \rangle)}}$$

where x_1, x_2,...x_{3N} are the mass-weighted Cartesian coordinates of an N-particle system and $\langle\rangle$ denotes the average over the trajectory. The DCCMs were generated for coarse-grained trajectories in which each residue from the atomistic MD simulations was represented by a bead at its center of mass. The analyses were performed using the GROMACS tools trjconv, g_covar, and g_anaeig.[43]

Free Energy Simulations. The free energy simulations were carried out using an approach that combines umbrella sampling with a finite temperature string method.[44,45] They were performed using the NAMD program package and the CHARMM22 force field[34] with the CMAP correction.[35] This approach to performing multidimensional free energy simulations of reaction processes can be outlined as follows.[45]

A reaction of interest is represented as a curve in an M-dimensional space, where M is a set of relevant reaction coordinates that describe the reaction. An initial string, constructed along a guess reaction pathway, is divided equally into N images, each of which has specific values of the M reaction coordinates. The phase space in the neighborhood of each image is then sampled by performing independent umbrella sampling MD simulations, with restraining potentials applied on the M reaction coordinates. After an appropriate simulation time the centers of the restraining potentials for each image are updated based on the average values of the reaction coordinates calculated from the restrained MD trajectories. A new string is then constructed from the updated centers of the restraining potential, which is then again divided equally into N new images. This process of updating the string based on restrained simulations is repeated until convergence, that is until the RMSD of the string between successive iterations falls below a certain threshold. Finally, the various biased trajectories from all the iterations are jointly unbiased using the weighted histogram analysis method to generate the M-dimensional free energy surface of the reaction. The converged string corresponds to the minimum free energy pathway of the reaction on the M-dimensional free energy surface.

We carried out independent sets of free energy simulations to explore the Gln182 conformational switch in the DS and LS species. To describe the Gln182 switch we chose two reaction coordinates, namely the CB(Gln182)—CG(Gln182)—CD(Gln182)—NE2-(Gln182) dihedral angle and the N5(FAD)—NE2(Gln182) distance. The initial and final states of the Gln182 switch for DS and LS are defined in the following. For both simulation sets the initial string was

DOI: 10.1021/jacs.6b10701
J. Am. Chem. Soc. 2017, 139, 2972−2980

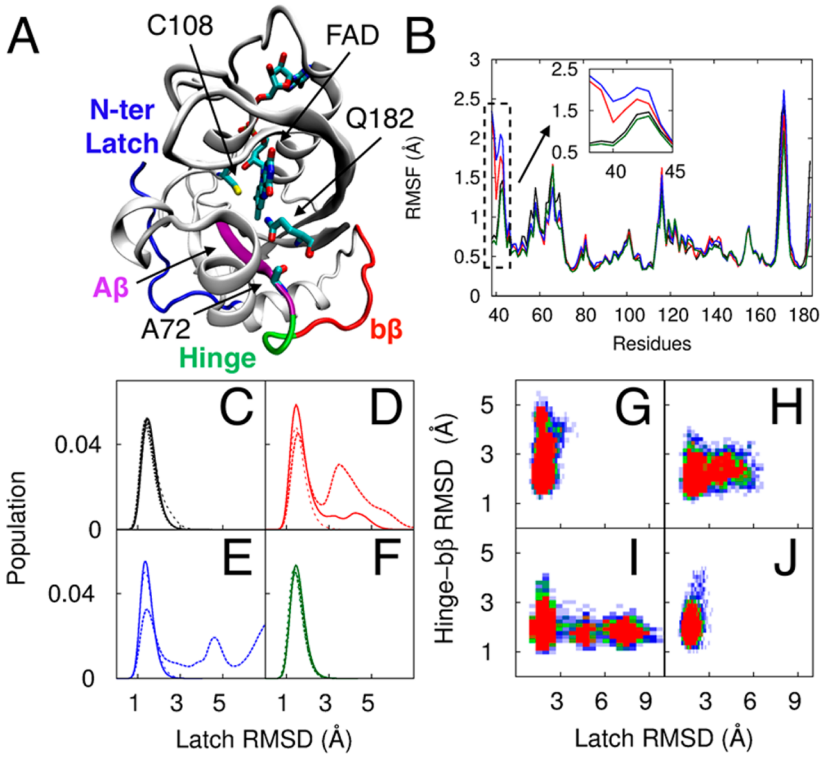

Figure 3. Dynamics of the N-terminal latch of the LOV domain along the VVD photocycle observed in MD simulations. (A) Crystal conformation of DS VVD with key residues and regions labeled [PDB ID 2PD7]. (B) Average RMSFs of residues of VVD in DS (black), LS (red), LAS (blue), and FADH (green); those of residues 38−45 in the N-terminal latch are highlighted in the inset. (C−F) Distribution of the latch RMSDs with respect to the crystal conformation of VVD in DS (C, black), LS (D, red), LAS, (E, blue), and FADH (F, green), with different line styles corresponding to the independent MD trajectories. (G−J) 2D probability densities (high-red; low-blue) of the correlation between latch RMSDs and RMSDs of residues in the hinge and bβ region (residues 62−71) for DS (G, black), LS (H, red), LAS (I, blue), and FADH (J, green). See text for discussion.

constructed from a linear interpolation between the two end states and 37 equally spaced images were considered along the respective strings. Each image was propagated for 100 and 500 ps per iteration for DS and LS respectively, and harmonic potentials with force constants of 0.1 to 0.3 kcal mol^{-1}A^{-2} were applied to the reaction coordinates. The total simulation times for the DS and LS sets of simulations per image were 4 and 9 ns, respectively.

RESULTS

To elucidate the signal transduction mechanism of VVD we carried out MD simulations of VVD in several states of the flavin cofactor and the protein conformation initially defined by the respective crystal structures.[10] The dark state (DS) is based on the crystal structure of the protein with oxidized flavin in the dark (Figure 1A,E). The light state (LS) contains the dark-state protein conformation and the cysteinyl flavin adduct taken from structures of light-exposed crystals (Figure 1A,B,E).[10] The light-adapted state (LAS) contains the adduct and includes the structural changes of the protein that occur when the dark-state crystals are illuminated (Figure 1A,B,E). In addition, we performed simulations of Cys-less VVD with the FAD chromophore in the neutral semiquinone radical state (FADH; Figure 1C,D). For each state, we propagated at least three 25 ns MD trajectories from different initial conditions.

To depict the Gln182 orientation with respect to the FAD moiety in the various MD simulations we follow the angle (denoted as α) formed by the vectors passing through the atoms CD and NE2 of Gln182 and the atoms N5 and N10 of FAD (Figure 2A). The angle α is close to zero when the CD—NE2 (Gln182) vector is parallel to the N5—N10 (FAD) vector, i.e. when Gln182 is facing FAD with its amine moiety, and it assumes a value close to 180° when the CD—NE2 (Gln182) vector is antiparallel to the N5—N10 (FAD) vector, i.e., when Gln182 is facing FAD with its carbonyl moiety. The Gln orientation is very sensitive to the VVD state as depicted by the evolution of α along the trajectories (Figures 2B−E with representative geometries of the active site in Figures 2F−H and RMSDs of the residue in Figure S1 of the Supporting Information). In DS, the conformational switch of Gln182 is never observed in any of the MD trajectories. The residue remains mostly close to its crystal orientation except in the later stage of one trajectory when it rotates out of its crystal position away from the FAD moiety (Figures 2B,F,G and S1). In LS and FADH, Gln182 remains localized initially in the active site as well, but at some point the Gln182 switch occurs in each trajectory, as indicated by the sudden jumps of α in Figure 2C,E and of the Gln182 RMSD in Figure S1. In LAS, the Gln182 is already switched, and thus remains stable close to its crystal conformation in all trajectories (Figures S1 and S2). The stability of the switched Gln182 conformation in the LS, LAS, and FADH states indicates that the conformation of Gln182 is strongly dependent on the oxidation and protonation state of FAD.

In the VVD activation pathway, the formation of the cysteinyl adduct is accompanied by the release of the N-terminal latch, which then interacts with another VVD subunit in the VVD dimer state.[13] We analyzed the motions of the latch in the various VVD states (Figure 3) to examine whether

DOI: 10.1021/jacs.6b10701
J. Am. Chem. Soc. 2017, 139, 2972−2980

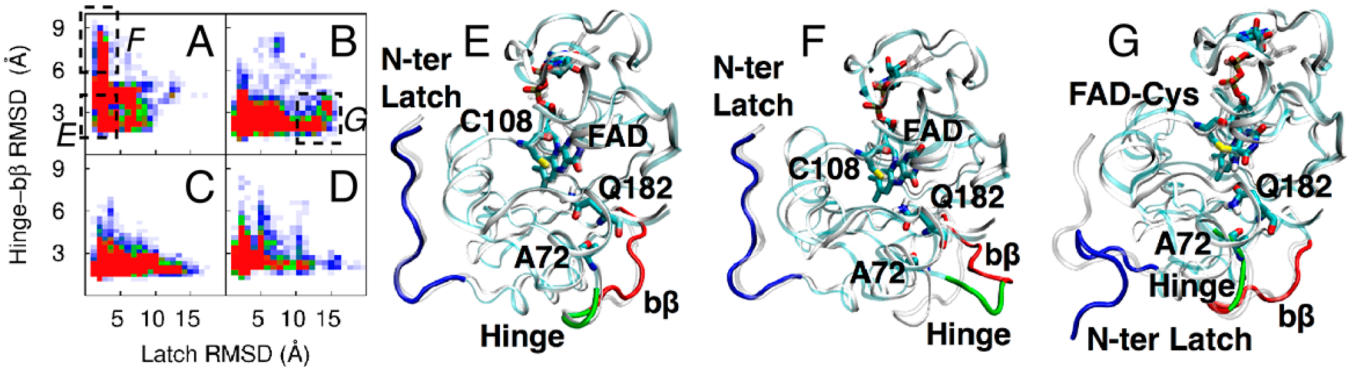

Figure 4. Anticorrelation between the motions of the N-terminal latch and hinge-bβ regions in the VVD LOV domain observed in REMD simulations. (A–D) 2D probability densities (high-red; low-blue) of the correlation between latch and hinge-bβ RMSDs in DS (A), LS (B), LAS (C), and FADH (D). (E–G) Representative conformations of DS (A) and LS (B) from the regions marked by the dotted boxes E–G in A and B. See text for discussion.

Gln182 communicates with this important signaling element (blue in Figures 1E and 3A). The average root-mean-square fluctuations (RMSFs) of the residues calculated from the various MD trajectories for all the VVD states (Figure 3B) show that the latch residues are more flexible in LS and LAS than in DS and FADH. The increased latch motion in LS and LAS is further illustrated by the RMSD distributions of the residues in the latch (residues 38 to 48), with respect to their crystal structure in each independent MD trajectory (Figure 3C–F). In DS, the latch is quite rigid and remains close to its crystal conformation in all trajectories (RMSD distributions with a single sharp peak close to 1 Å in Figure 3C); in LS and LAS, the latch opens in some trajectories, as indicated by the broad RMSD distributions (Figure 3D,E). In FADH, the dynamical behavior of the latch is similar to that of DS, mostly rigid and close to the crystal structure (Figure 3F).

The dynamics of the N-terminal latch and the hinge-bβ region of the Ncap (red, Figure 3A) show an interesting anticorrelation (Figure 3G–J). The hinge-bβ region comprises a single strand of mostly β backbone geometry that packs against both the PAS β-sheet and the Aα Ncap helix (Figures 1E and 3A). Interestingly, the hinge-bβ region (residues 62 to 71) is more flexible in DS and FADH than in LS and LAS. In DS and FADH (Figures 3G,J) the conformations sampled are characterized by low latch RMSDs and high hinge-bβ RMSDs, whereas the opposite is found in LS and LAS (Figure 3H,I). This anticorrelation may reflect the enhanced hydrogen bonding between the Gln182 amine and the Ala72 carbonyl group of the Aβ backbone when the Gln amide flips in response to flavin protonation (Figure S2). The bβ region immediately precedes the hinge that connects the Ncap to Aβ of the PAS domain.

The N-terminal latch release is a rather large conformational change that may not be adequately sampled in traditional MD simulations owing to the inherent well-known sampling limitations of the method. In an effort to improve the sampling of the free energy landscape of VVD, we performed extensive REMD simulations for the different VVD states. These simulations largely support the results from the standard MD trajectories. In DS, the Gln182 orientation, as described by the angle α (Figure 2A), is broad and centered around 30° (Figure S3A), which indicates that the Gln182 faces FAD mostly with its amine. The breadth of the distribution reflects the flexibility of Gln182 in DS in that the side chain often rotates out from its active site position away from the FAD, as also observed in the DS MD trajectories (Figure 2G). This conformational change is further reflected in the RMSD distribution of Gln182, which is broad and consists of two distinct peaks (Figure S3B). The first peak, centered close to 1 Å, corresponds to configurations in which Gln182 remains close to its crystal conformation and faces FAD with its amine (Figure 2F). The second peak, centered around 3 Å, represents a population in which Gln182 is rotated out of the active site. For the states LS and FADH, the distribution of α exhibits a sharper peak centered around ~150° (Figure S3A) and the Gln182 RMSD distribution has a sharp peak at a value slightly higher than 1 Å (Figure S3B). These data indicate that LS and FADH favor a Gln182 conformation with the carbonyl oriented toward FAD that is also much less mobile than in DS. For LAS, the distribution of α shows a sharp peak at around ~150° (Figure S3A) and the Gln182 RMSD distribution reveals a single, albeit a less sharp peak at a value slightly lower than 1 Å (Figure S3B). Thus, in the LAS state Gln182 remains close to the crystal conformation, with Gln182 carbonyl facing the FAD, but it is somewhat more flexible than in the LS and FADH states. Time traces of α in the various REMD simulations (Figure S4) indicate that in each case the Gln182 conformational switch occurs several times, thus suggesting that an accessible free energy barrier connects the state in which Gln182 faces FAD with its amine to the state in which the residue faces FAD with its carbonyl.

The REMD simulations confirm the correlations among the motions of the N-terminal latch, the orientation of the Gln182 side chain, and the motions of the hinge-bβ region that are observed in the MD trajectories. The residues corresponding to the N-terminal latch are found to be much more flexible for LS and LAS than for DS and FADH (Figure S5A). The distributions of the latch RMSDs from the REMD simulations for DS show that the bulk of conformations have latch RMSDs less than 5 Å (Figure S5B) and only a small fraction of conformations have latch RMSDs greater than 10 Å. By contrast, the corresponding distributions for LS and LAS indicate significant populations of conformations with latch RMSDs greater than 10 Å (Figure S5C,D). In FADH, the latch is mostly rigid during the MD simulations, but there is also a substantial population of configurations with latch RMSDs greater than 10 Å (Figure S5E). Thus, the REMD simulations support latch opening in FADH and thereby further strengthen the correlation between Gln182 conformation and latch motion.

DOI: 10.1021/jacs.6b10701
J. Am. Chem. Soc. 2017, 139, 2972–2980

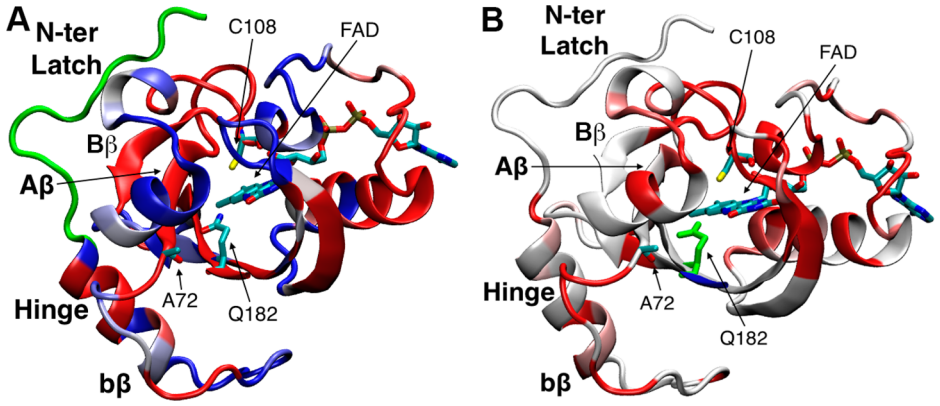

Figure 5. Correlated motions in VVD obtained from the DCCMs. (A) Regions of VVD are colored according to the extent of their absolute correlation to the N-terminal latch (latch in green; red—most correlation, blue—least correlation). (B) Motional correlations of Gln182 to various VVD regions. In this case, negative correlations are shown in red, positive in blue. DCCMs were constructed from the independent concatenated trajectories of the DS. See also Table S1.

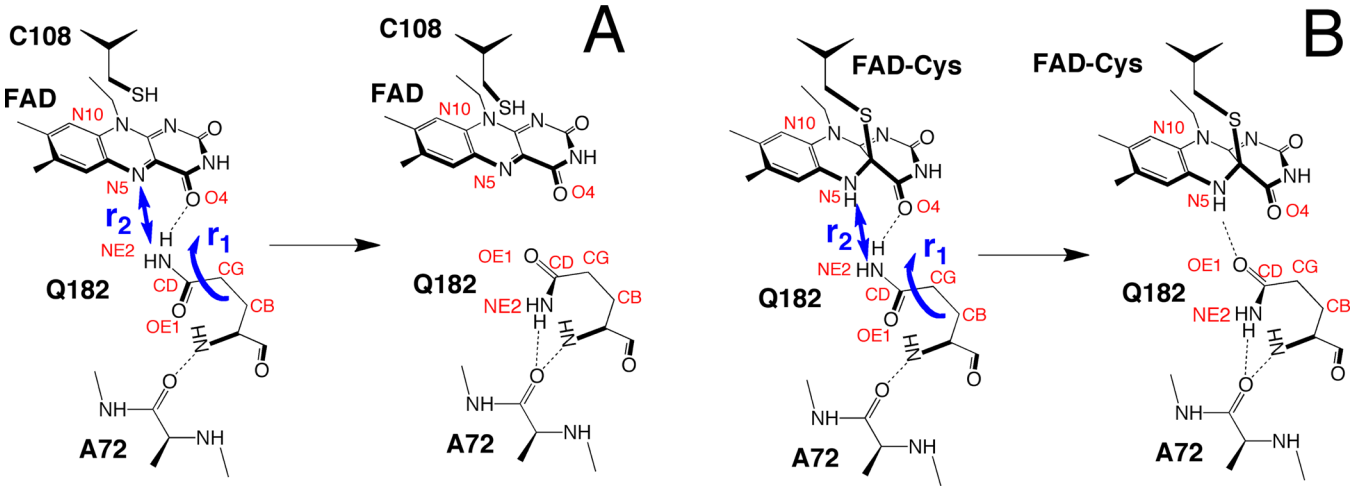

Figure 6. Transformations in DS (A) and LS (B) studied using string simulations. At the beginning Gln182 is facing FAD with its amide, and at the end Gln182 has switched and is facing FAD with its carbonyl. The CB-CG-CD-NE2 dihedral angle of Gln182 (denoted as r_1) and the distance between NE2 (Gln182) and N5 (FAD) (denoted as r_2) are selected as reaction coordinates.

The REMD simulations also underscore the inverse relationship between the motions of the latch and the hinge-bβ region. The residues in the hinge-bβ region were found to be more mobile in DS than in LS, LAS, and FADH (Figure S5A). The latch and the hinge-bβ RMSDs obtained from the REMD simulations are again anticorrelated in the various VVD states (Figure 4). DS has significant population of conformations with low latch RMSDs and high hinge-bβ RMSDs, and almost no conformations with high latch RMSDs and low hinge RMSDs (Figure 4A). Representative DS conformations with low latch RMSDs and low hinge-bβ RMSDs closely resemble the crystal structure (Figure 4E), whereas those with low latch RMSDs and high hinge-bβ RMSDs exhibit large fluctuations of bβ toward the last PAS β-strand Iβ (Figure 4F). By contrast, the behaviors of LS, LAS, and FADH are similar in that there is significant population in the region of high latch RMSDs and low hinge-bβ RMSDs, and no population in the region of low latch RMSDs and high hinge-bβ RMSDs. A representative conformation of LS with high latch RMSDs-low hinge RMSDs contains a latch region largely displaced from the protein core (Figure 4G).

To further investigate correlated motions in VVD, we generated dynamic cross-correlation maps (DCCMs) for the various MD and REMD trajectories (Figures 5, S6, and S7). A DCCM obtained from the DS MD trajectories identifies the different regions of VVD that are highly correlated to the latch (Figures 5A and S6A), including the hinge-bβ region and the N-terminal β-strands of the core PAS domain (Aβ and Bβ), against which the latch binds in the DS. Absolute correlations of the hinge-bβ residues to the latch are generally larger in the REMD simulations compared to the MD simulations and are the greatest in the LAS state (Table S1). This trend may reflect the fact that even though the latch is unreleased in the LAS starting geometry, the relatively minor conformational changes that distinguish the LAS from the LS are along the proper progression to the true light-activated conformation. It follows that the REMD simulations are better able to reproduce this trajectory from the LS than the MD simulations. Interestingly, movements of Gln182 itself are highly correlated with the hinge-bβ region, but not greatly with the latch itself (Figure 5B). Furthermore, motions of Ncap helix aα that connects hinge-bβ to the latch are also correlated with motions of Gln182. Thus, despite the many motional correlations observed throughout the structure, it is the hinge-bβ region that appears to couple Gln182 rearrangement to latch movement.

DOI: 10.1021/jacs.6b10701
J. Am. Chem. Soc. 2017, 139, 2972−2980

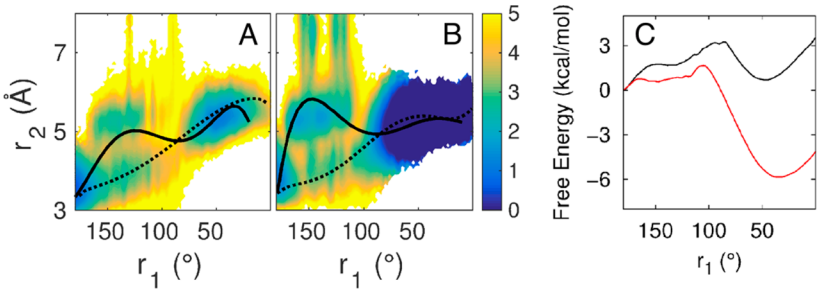

Figure 7. Free energy calculations for the Gln182 switch in VVD. (A,B) 2D free energy surfaces of the Gln182 switch obtained from the string simulations for VVD in DS (A) and LS (B) using the reaction coordinates r_1 and r_2 defined in Figure 5; the dotted and solid black lines correspond to the initial and converged strings, respectively. (C) 1D free energy profiles of the Gln182 switch in DS (black) and LS (red) obtained by projecting the corresponding 2D surfaces along the r_1 reaction coordinate. See text for discussion.

The MD simulations establish that the Gln182 switch is a key conformational response to flavin adduct formation. Hence, we investigated the ease of this transformation in the DS and LS states of VVD by performing free energy simulations for the two states. The simulations were carried out by combining umbrella sampling with a finite temperature string method. This approach[44,45] (see Methods section and Figure S8) was used to investigate the transformations illustrated in Figure 6. The Gln182 switch was described by two reaction coordinates, namely the CB-CG-CD-NE2 (Gln182) dihedral angle (denoted as r1) and the NE2(Gln182)-N5(FAD) distance (denoted as r2). At the beginning, Gln182 is facing FAD with its amine, hence r1 ∼180° and r2 ∼3 Å, and at the end, Gln182 is facing FAD with its carbonyl, hence r1 ∼0° and r2 ∼5 Å.

The 2D free energy surfaces computed for the Gln182 switch in the DS and LS states along reaction coordinates r1 and r2 are shown in Figure 7A,B, respectively, and the respective 1D free energy profiles along r1 are depicted in Figure 7C. The 2D and 1D free energy profiles indicate that in DS the free energy barrier of the switch is ∼3.2 kcal/mol and that the pre- and postswitch states are almost equally favorable, with the final state being higher in free energy by ∼0.7 kcal/mol. The free energy profiles also indicate the presence of a shallow intermediate corresponding to conformations previously observed in MD simulations (Figure 7) where the Gln182 rotates out of the active site away from the FAD. The free energy barrier to this intermediate state is ∼2.8 kcal/mol making it accessible to the MD simulations, albeit on rare occasions. The free energy profiles yield a barrier for the Gln182 switch in LS of only ∼1.7 kcal/mol, explaining why the switch is observed in every MD trajectory. More importantly, the postswitch state is much more favorable than the preswitch state (by ∼6 kcal/mol), which accounts for the stability of the Gln182 conformation after the switch has occurred. The LS state also features a shallow intermediate (as in DS). However, the free energy barriers for accessing and leaving this state are less than 0.5 kcal/mol, so that the postswitch conformation remains heavily favored in the MD simulations.

DISCUSSION

The MD simulations of VVD agree very well with experiment. Protonation of the flavin N5 in either the adduct state or the neutral semiquinone state causes a flipping of the Gln182 amide group. Consistent with the crystal structures,[10,13] this motion causes a new hydrogen bond to form between the Ala72 carbonyl and the Gln182 amide, thus increasing the number of hydrogen bonds between Gln182 and Aβ from one to two (a main-chain hydrogen bond between the Gln182 carbonyl and the Ala72 peptide amide is maintained in all states). This new hydrogen bond appears to stabilize the hinge to the Ncap, which in turn reduces the dynamics of the nearby bβ strand. Notably, the structure of VVD from dark-grown crystals, illuminated and trapped at low temperature, shows movement of bβ upon adduct formation.[10] The MD simulations also reveal that the stabilization of the bβ strand is anticorrelated with the dynamics of the N-terminal latch, which in the Gln182 flipped state releases from the protein core in agreement with the known influence of the N-terminus on dimerization[24] and the structure of the light-activated VVD dimer.[13] VVD dimerization, which is key for function, depends on the latch disengaging from its position against the PAS core to bind the opposing subunit. It is satisfying that these key elements of activation are recapitulated in the simulations.

Flipping of the Gln amide is observed both in the case of adduct formation and of flavin semiquinone formation (FADH). Because both flavin states induce VVD dimerization and stimulate biological activity, it is reasonable that both should cause the same immediate response from the protein environment. The changes in hydrogen bonding of the flavin revealed in the simulations are supported by FTIR measurements on other LOV proteins. For example, FTIR spectra of LOV2 from photochrome3 exhibit an upshift in the flavin C(4)=O4 vibrational frequency attributable to loss of hydrogen bonding in either the adduct state or when the conserved Gln is substituted for Leu.[20] The simulations clearly show the loss of Gln hydrogen bonding to the flavin carbonyl on transition to the LAS (Figure S2). Time resolved FTIR data on phototropin LOV2 indicate a similar effect on the flavin carbonyl, but also find changes in a likely Gln side-chain resonance that evolves on the same time scale as adduct formation.[23]

Importantly, our work provides information on the free energy landscape associated with Gln flipping. A shallow intermediate precedes the transition state to Gln182 flipping in both DS and LS, which corresponds to a partially rotated Gln side chain, as observed in the DS simulations. However, the free energy barrier for crossing to the flipped conformation is ∼1.5 kcal/mol lower in LS compared with DS. In systems where this has been measured, LOV proteins have much higher energy in their adduct states (by more than 40 kcal/mol).[46] This energy may be harnessed to enable small motions that better accommodate the Gln flip, and again the presence of the N5 hydrogen may have an influence on the TS. The free energy profiles clearly show that the Gln reorientation is highly favored in LS; the postswitch conformation is much lower in free

DOI: 10.1021/jacs.6b10701
J. Am. Chem. Soc. 2017, 139, 2972−2980

energy than the preswitch conformation owing to the favorable interactions between the Gln182 amide and the Ala72 carbonyl, and between the Gln182 carbonyl and the flavin N5−H.

The MD results reported here contrast with a previous MD study of the dark (DS) and light (LS) states of the VVD LOV domain.[26] In that work, the LS exhibited large-scale motions of Gln182 with the side chain moving out of its crystal structure position to a conformation devoid of interactions with the FAD isoalloxazine ring and Ala72. These previous observations[26] were, however, based on only a single 20 ns MD trajectory. Furthermore, the simulation was performed using the "non-invasive thermostating technique", in which the protein and the flavin moiety were decoupled from the thermostat (Nosé−Hoover) in an effort to sample configurations that are far from equilibrium. It seems possible that this strategy overemphasized large-scale conformational changes at the expense of more subtle ones such as the Gln flip.[26] Similar simulations on AsPhot1-LOV2 by analogous methods suggested that the breakage of the Q497-D540 and Q479-E518 hydrogen bonds plays a role in Jα dissociation,[47] which is inconsistent with experimental data on AsPhot1-LOV2 mutants in which one partner from each of these interactions was removed with little effect on activity.[48] More recently, the dark and light states of the AsPhot1-LOV2 domain were investigated using longer (200 ns) MD simulations.[25] In these simulations putative Jα predissociation states were observed and the Jα dissociation was linked to the conformation of the FAD binding site, more specifically to the conformation of the analogous Gln513. In the dark state, Gln513 resided predominantly in a position close to, but somewhat different from the crystal conformation. In the light state, Gln513 populated a wide range of conformations in which the residue rotated out from its crystal position away from the FAD isoalloxazine to varying degrees. Interestingly, these Gln513 conformations are similar to those observed in this study, most frequently in the DS simulations and rarely in the LS, LAS, and FADH simulations.

It is certainly possible that all LOV domains do not behave the same, and variations in the response of the conserved Gln depend on the coupling with different neighboring residues and more extensive nonconserved elements, such as the Ncap and Ccap regions. Nonetheless, in virtually all studies the invariant Gln residue is proposed to respond to adduct formation. For VVD, these changes involve a rotary flip of the Gln amide side chain, induced primarily by protonation of flavin N5. A newly formed hydrogen bond between the reoriented Gln and the N-terminus of Aβ then stabilizes the proximate regions of the Ncap, which in turn destabilize the N-terminal latch against the protein core, allowing for its release.

The cross-correlation analysis provides new insight into this activation mechanism. Not surprisingly, latch motion is correlated with motions in many other regions of the protein, largely due to the extensive interactions between the latch and the core β-sheet. However, motions of Aβ and neighboring Bβ correlate with those of the latch, but not with those of Gln182. Thus, changes in the core β-sheet more likely reflect latch release than conformational propagation through the β-sheet from Gln182. In contrast, it is very interesting that dynamics in both Gln182 and the latch correlate with those of hinge-bβ, even though Gln182 is uncorrelated to the latch itself. Hence, hinge-bβ, which is directly affected by the new hydrogen bond to Ala72 upon Gln182 rearrangement, couples conformational changes responding to flavin protonation state (i.e., Gln182) to the dynamics of a recognition motif at the protein surface (i.e., the latch).

Our study also reveals an anticorrelation between the magnitude of the dynamics of the hinge-bβ and those of the latch, which suggests that it is stabilization of the hinge-bβ that then destabilizes the latch against the PAS core. Opposing stabilities of coupled adjacent structural elements is an emerging theme in signal propagation. For example, in bacterial chemoreceptors sequential domains appear to undergo alternating changes in dynamics and/or stability as the receptors switch between off and on states.[49] This so-called "yin-yang" behavior[50] allows the influence of one region onto another in that the two interacting units cannot both be simultaneously "stable". Similar properties have been found for adenylate cyclases, where the unfolding of a linker region releases the catalytic cores to engage and become active.[51] Less dramatic, but consistent behavior is seen in BLUF-domain linked phosphodiesterases, in which the dynamics of the light-sensing BLUF domain and the catalytic phosphodiesterase domain also appear to be anticorrelated.[52] In general, alternating the stability of successively coupled structural regions is an attractive means to propagate long-range signals in modular systems because it does not necessarily depend on unique types of residue interactions, and shifts in the energetics can roughly balance throughout the linked modules.

CONCLUSIONS

All-atom MD and REMD simulations of the VVD photoreceptor in different flavin chemical states reproduce key conformational changes associated with the light activation process that are observed experimentally. The simulations provide an atomistic picture underlying the flipping of Gln182 in response to flavin N5 protonation and subsequent release of the N-terminal latch from the PAS domain core. Free-energy calculations quantitatively evaluate the feasibility of a Gln flip in the dark and light states of VVD and thereby indicate that the free energy barrier to this rearrangement is lower and thermally accessible in the flavin adduct state (light state). The simulations also reveal an anticorrelation between the dynamics of a hinge-bβ element and the N-terminal latch that transduces alternations in flavin hydrogen bonding to larger-scale conformational changes at the protein N-terminus. Thus, our study lends computational support to a general signal transduction mechanism that involves competition between the dynamics of coupled structural regions.

ASSOCIATED CONTENT

Supporting Information

The Supporting Information is available free of charge on the ACS Publications website at DOI: 10.1021/jacs.6b10701.

RMSDs of Gln182 with respect to crystal structures; hydrogen bonding patterns in VVD active site; Gln182 conformations from REMD simulations; dynamics of N-terminal latch from REMD simulations; DCCMs of VVD from MD and REMD simulations; correlation coefficients for latch hinge-bβ motions; convergence of string simulations; and flavin force-field parameters (PDF)

AUTHOR INFORMATION

Corresponding Author

*bc69@cornell.edu

DOI: 10.1021/jacs.6b10701
J. Am. Chem. Soc. 2017, 139, 2972−2980

ORCID

Walter Thiel: 0000-0001-6780-0350
Brian R. Crane: 0000-0001-8234-9991

Notes

The authors declare no competing financial interest.

■ ACKNOWLEDGMENTS

This work was supported by NIH Grant GM079679 and a fellowship from the John Simon Guggenheim foundation (to B.R.C.).

■ REFERENCES

(1) Conrad, K. S.; Manahan, C. C.; Crane, B. R. *Nat. Chem. Biol.* **2014**, *10*, 801−809.
(2) Losi, A.; Gärtner, W. *Photochem. Photobiol.* **2011**, *87*, 491−510.
(3) Zoltowski, B. D.; Gardner, K. H. *Biochemistry* **2011**, *50*, 4−16.
(4) Crosson, S.; Rajagopal, S.; Moffat, K. *Biochemistry* **2003**, *42*, 2−10.
(5) Kennis, J. T. M.; Groot, M. L. *Curr. Opin. Struct. Biol.* **2007**, *17*, 623−630.
(6) Losi, A. *Photochem. Photobiol.* **2007**, *83*, 1283−1300.
(7) Crosson, S.; Moffat, K. *Plant Cell* **2002**, *14*, 1067−1075.
(8) Fedorov, R.; Schlichting, I.; Hartmann, E.; Domratcheva, T.; Fuhrmann, M.; Hegemann, P. *Biophys. J.* **2003**, *84*, 2474−2482.
(9) Nash, A. I.; Ko, W. H.; Harper, S. M.; Gardner, K. H. *Biochemistry* **2008**, *47*, 13842−13849.
(10) Zoltowski, B. D.; Schwerdtfeger, C.; Widom, J.; Loros, J. J.; Bilwes, A. M.; Dunlap, J. C.; Crane, B. R. *Science* **2007**, *316*, 1054−1057.
(11) Crosson, S.; Moffat, K. *Proc. Natl. Acad. Sci. U. S. A.* **2001**, *98*, 2995−3000.
(12) Moglich, A.; Moffat, K. *J. Mol. Biol.* **2007**, *373*, 112−126.
(13) Vaidya, A. T.; Chen, C. H.; Dunlap, J. C.; Loros, J. J.; Crane, B. R. *Sci. Signal.* **2011**, *4*, ra50 DOI: 10.1126/scisignal.2001945.
(14) Endres, S.; Granzin, J.; Circolone, F.; Stadler, A.; Krauss, U.; Drepper, T.; Svensson, V.; Knieps-Grunhagen, E.; Wirtz, A.; Cousin, A.; Tielen, P.; Willbold, D.; Jaeger, K. E.; Batra-Safferling, R. *BMC Microbiol.* **2015**, *15*, 30 DOI: 10.1186/s12866-015-0365-0.
(15) Hisatomi, O.; Takeuchi, K.; Zikihara, K.; Ookubo, Y.; Nakatani, Y.; Takahashi, F.; Tokutomi, S.; Kataoka, H. *Plant Cell Physiol.* **2013**, *54*, 93−106.
(16) Halavaty, A. S.; Moffat, K. *Biochemistry* **2007**, *46*, 14001−14009.
(17) Röllen, K.; Granzin, J.; Panwalkar, V.; Arinkin, V.; Rani, R.; Hartmann, R.; Krauss, U.; Jaeger, K.-E.; Willbold, D.; Batra-Safferling, R. *J. Mol. Biol.* **2016**, *428*, 3721−3736.
(18) Losi, A.; Ghiraldelli, E.; Jansen, S.; Gärtner, W. *Photochem. Photobiol.* **2005**, *81*, 1145−1152.
(19) Yee, E. F.; Diensthuber, R. P.; Vaidya, A. T.; Borbat, P. P.; Engelhard, C.; Freed, J. H.; Bittl, R.; Moeglich, A.; Crane, B. R. *Nat. Commun.***2015**, *6*, 10.1038/ncomms10079.
(20) Nozaki, D.; Iwata, T.; Ishikawa, T.; Todo, T.; Tokutomi, S.; Kandori, H. *Biochemistry* **2004**, *43*, 8373−8379.
(21) Raffelberg, S.; Mansurova, M.; Gärtner, W.; Losi, A. *J. Am. Chem. Soc.* **2011**, *133*, 5346−5356.
(22) Jones, M. A.; Feeney, K. A.; Kelly, S. M.; Christie, J. M. *J. Biol. Chem.* **2006**, *282*, 6405−6414.
(23) Pfeifer, A.; Majerus, T.; Zikihara, K.; Matsuoka, D.; Tokutomi, S.; Heberle, J.; Kottke, T. *Biophys. J.* **2009**, *96*, 1462−1470.
(24) Zoltowski, B. D.; Crane, B. R. *Biochemistry* **2008**, *47*, 7012−7019.
(25) Freddolino, P. L.; Gardner, K. H.; Schulten, K. *Photochem. Photobiol. Sci.* **2013**, *12*, 1158−1170.
(26) Peter, E.; Dick, B.; Baeurle, S. A. *Proteins: Struct., Funct., Genet.* **2012**, *80*, 471−481.
(27) Jorgensen, W. L.; Chandrasekhar, J.; Madura, J. D.; Impey, R. W.; Klein, M. L. *J. Chem. Phys.* **1983**, *79*, 926−935.
(28) Darden, T.; York, D.; Pedersen, L. *J. Chem. Phys.* **1993**, *98*, 10089−10092.
(29) Ryckaert, J.-P.; Ciccotti, G.; Berendsen, H. J. C. *J. Comput. Phys.* **1977**, *23*, 327−341.
(30) Nosé, S. *Mol. Phys.* **1984**, *52*, 255−268.
(31) Martyna, G. J.; Tobias, D. J.; Klein, M. L. *J. Chem. Phys.* **1994**, *101*, 4177−4189.
(32) Feller, S. E.; Zhang, Y.; Pastor, R. W.; Brooks, B. R. *J. Chem. Phys.* **1995**, *103*, 4613−4621.
(33) Phillips, J. C.; Braun, R.; Wang, W.; Gumbart, J.; Tajkhorshid, E.; Villa, E.; Chipot, C.; Skeel, R. D.; Kalé, L.; Schulten, K. *J. Comput. Chem.* **2005**, *26*, 1781−1802.
(34) MacKerell, A. D.; Bashford, D.; Bellott, M.; Dunbrack, R. L.; Evanseck, J. D.; Field, M. J.; Fischer, S.; Gao, J.; Guo, H.; Ha, S.; Joseph-McCarthy, D.; Kuchnir, L.; Kuczera, K.; Lau, F. T. K.; Mattos, C.; Michnick, S.; Ngo, T.; Nguyen, D. T.; Prodhom, B.; Reiher, W. E.; Roux, B.; Schlenkrich, M.; Smith, J. C.; Stote, R.; Straub, J.; Watanabe, M.; Wiórkiewicz-Kuczera, J.; Yin, D.; Karplus, M. *J. Phys. Chem. B* **1998**, *102*, 3586−3616.
(35) Mackerell, A. D.; Feig, M.; Brooks, C. L. *J. Comput. Chem.* **2004**, *25*, 1400−1415.
(36) Luo, G.; Andricioaei, I.; Xie, X. S.; Karplus, M. *J. Phys. Chem. B* **2006**, *110*, 9363−9367.
(37) Bayly, C. I.; Cieplak, P.; Cornell, W.; Kollman, P. A. *J. Phys. Chem.* **1993**, *97*, 10269−10280.
(38) Hukushima, K.; Nemoto, K. *J. Phys. Soc. Jpn.* **1996**, *65*, 1604−1608.
(39) Okabe, T.; Kawata, M.; Okamoto, Y.; Mikami, M. *Chem. Phys. Lett.* **2001**, *335*, 435−439.
(40) Patriksson, A.; van der Spoel, D. *Phys. Chem. Chem. Phys.* **2008**, *10*, 2073−2077.
(41) Parrinello, M.; Rahman, A. *J. Appl. Phys.* **1981**, *52*, 7182−7190.
(42) Parrinello, M.; Rahman, A. *J. Chem. Phys.* **1982**, *76*, 2662−2666.
(43) Van Der Spoel, D.; Lindahl, E.; Hess, B.; Groenhof, G.; Mark, A. E.; Berendsen, H. J. C. *J. Comput. Chem.* **2005**, *26*, 1701−1718.
(44) Rosta, E.; Nowotny, M.; Yang, W.; Hummer, G. *J. Am. Chem. Soc.* **2011**, *133*, 8934−8941.
(45) Ganguly, A.; Thaplyal, P.; Rosta, E.; Bevilacqua, P. C.; Hammes-Schiffer, S. *J. Am. Chem. Soc.* **2014**, *136*, 1483−1496.
(46) Losi, A.; Kottke, T.; Hegemann, P. *Biophys. J.* **2004**, *86*, 1051−1060.
(47) Peter, E.; Dick, B.; Baeurle, S. A. *J. Chem. Phys.* **2012**, *136*, 124112.
(48) Zayner, J. P.; Antoniou, C.; Sosnick, T. R. *J. Mol. Biol.* **2012**, *419*, 61−74.
(49) Parkinson, J. S.; Hazelbauer, G. L.; Falke, J. J. *Trends Microbiol.* **2015**, *23*, 257−266.
(50) Swain, K. E.; Falke, J. J. *Biochemistry* **2007**, *46*, 13684−13695.
(51) Tews, I.; Findeisen, F.; Sinning, I.; Schultz, A.; Schultz, J. E.; Linder, J. U. *Science* **2005**, *308*, 1020.
(52) Winkler, A.; Udvarhelyi, A.; Hartmann, E.; Reinstein, J.; Menzel, A.; Shoeman, R. L.; Schlichting, I. *J. Mol. Biol.* **2014**, *426*, 853−868.

DOI: 10.1021/jacs.6b10701
J. Am. Chem. Soc. 2017, 139, 2972−2980